catalysts

MDPI

Article

MPV Reduction of Furfural to Furfuryl Alcohol on Mg, Zr, Ti, Zr–Ti, and Mg–Ti Solids: Influence of Acid–Base Properties

Jesús Hidalgo-Carrillo, Almudena Parejas, Manuel Jorge Cuesta-Rioboo, Alberto Marinas * and Francisco José Urbano

Departamento de Química Orgánica, Instituto Universitario de Investigación en Química Fina y Nanoquímica IUIQFN, Universidad de Córdoba, Campus de Rabanales, Edificio Marie Curie, E-14071 Córdoba, Spain; yimo@hotmail.com (J.H.-C.); q12pabaa@uco.es (A.P.); qo2maara@uco.es (M.J.C.-R.); qo1urnaf@uco.es (F.J.U.)
* Correspondence: alberto.marinas@uco.es; Tel.: +34-957-218-622

Received: 1 October 2018; Accepted: 9 November 2018; Published: 13 November 2018

Abstract: The Meerwein–Ponndorf–Verley (MPV) reaction is an environmentally-friendly process consisting of the reduction of a carbonyl compound through hydrogen transfer from a secondary alcohol. This work deals with MPV reduction of furfural to furfuryl alcohol on different ZrO_x, MgO_x, TiO_x, and Mg–Ti, as well as Zr–Ti mixed systems. The solids were synthesized through the sol–gel process and subsequently calcined at 200 °C. Characterization was performed using a wide range of techniques: ICP-MS, N_2 adsorption-desorption isotherms, EDX, TGA-DTA, XRD, XPS, TEM, TPD of pre-adsorbed pyridine (acidity) and CO_2 (basicity), DRIFT of adsorbed pyridine, and methylbutynol (MBOH) test reaction. ZrO_x showed the highest conversion and selectivity values, which was attributed to the existence of acid–base pair sites (as evidenced by the MBOH test reaction), whereas the introduction of titanium resulted in the drop of both conversion and selectivity probably due to the increase in Brönsted-type acidity. As for MgO_x, it had a predominantly basic character that led to the production of the condensation product of one molecule of furfural and one molecule of acetone, and thus resulted in a lower selectivity to furfuryl alcohol. The TiO_x solid was found to be mainly acidic and exhibited both Lewis and Brönsted acid sites. The presence of the latter could account for the lower selectivity to furfuryl alcohol. All in all, these results seemed to suggest that the MPV reaction is favored on Lewis acid sites and especially on acid–base pair sites. The process was accelerated under microwave irradiation.

Keywords: furfural; MPV reaction; acid–base characterization; methylbutynol test reaction

1. Introduction

The transformation of natural residues from agriculture into platform molecules is one of the promising research lines in obtaining high added value chemical products [1,2]. One of those platform molecules is furfural [3], which can be obtained from lignocellulose [4]. It contains an aromatic ring and an aldehyde group which makes it a versatile molecule to obtain a wide range of chemical compounds [5], and one of the most important ones is furfuryl alcohol. This alcohol is widely used in the production of thermostatic resins, rubbers, fibers, adhesives, and some fine chemicals [5–7]. Furfuryl alcohol is mainly produced by furfural hydrogenation. Approximately 60% of the furfural produced is used to synthesize furfuryl alcohol. The catalytic liquid-phase hydrogenation of furfural to produce furfuryl alcohol has been extensively investigated in the presence of catalysts based on Ni, Co, Cu, Pt, and Pd [8–12]. Cu–Cr-based catalysts are commonly used in the industry, but environmentally friendlier catalysts are required. The transformation of furfural to furfuryl alcohol can also be carried

out through the hydrogen transfer from a donor, which are typically secondary alcohols such as propan-2-ol, using the so-called Meerwein–Ponndorf–Verley (MPV) process [13]. This reaction involves the formation of a six-membered ring transition state in which both the reducing alcohol and the carbonyl compound are coordinated to the metal center (Lewis site) [14]. The assistance of the basic sites has also been proposed for the formation of the six-membered ring [15].

A wide range of heterogeneous catalysts has been described for the MPV process such as zirconia [16,17], mesoporous silica [18,19], zeolites [20], and alumina [21,22].

In previous papers, our research group described that zirconium gels calcined at low temperatures (ca. 200 °C) were quite selective to the corresponding unsaturated alcohol [16,17] in the MPV process. In the present work, different gels consisting of pure ZrO_x, TiO_x, and MgO_x, or mixed Mg–Ti and Zr–Ti solids and calcined at 200 °C were synthesized and tested in the MPV reduction of furfural to furfuryl alcohol to try and cast further light on the nature of the active sites responsible for the desired catalytic activity. The possibility of carrying out the reaction with microwave-assisted heating was also evaluated.

2. Results and Discussion

2.1. Textural, Structural, and Acid–Base Characterization of the Solids

The Brunnauer–Emmett–Teller (BET) surface areas as well as Mg/Ti and Zr/Ti atomic ratios (both nominal and experimental) of the synthesized solids are depicted in Table 1. The highest BET areas (in the 219–263 m^2/g range) corresponded to solids consisting of Zr and/or Ti, whereas lower values were found for the systems containing magnesium (42–81 m^2/g). In regard to the chemical composition, experimental results were in general quite similar to the nominal values and was thus evidence of a good precipitation of the metals during the synthesis.

Table 1. Brunnauer–Emmett–Teller (BET) surface area and atomic composition (nominal and experimental) of the different solids synthesized in the present study.

Catalyst	BET Surface Area (m^2/g)	M/Ti Ratio (M = Zr or Mg)		
		Nominal	ICP-MS	XPS
ZrO_x	221	-	-	-
Zr3Ti1	251	3.0	2.43	2.29
ZrTi	263	1.0	0.78	1.03
Zr1Ti3	219	0.33	0.34	0.45
TiO_x	232	-	-	-
Mg1Ti3	42	0.33	0.45	0.39
MgTi	81	1.0	1.06	0.62
Mg3Ti1	68	3.0	3.02	3.5
MgO_x	66	-	-	-

The TGA-DTA profiles of the different solids are shown in Figures 1 and 2 (Zr–Ti and Mg–Ti solids, respectively). The ZrO_x heat flow profile (Figure 1B) exhibited two main peaks centered at ca. 104 °C and 436 °C, respectively. The first endothermal peak corresponded to the loss of water whereas the second peak was the so-called glow exotherm attributed to the crystallization of zirconia [17,23]. For Zr–Ti mixed systems, the glow-exotherm was shifted to higher temperatures (450–466 °C) which suggests that titanium retards zirconium crystallization. In the case of MgO_x solids (Figure 2B), the heat flow profile exhibited two main endothermal peaks centered at ca. 117 °C and 385 °C. The latter peak was assigned to the transformation of $Mg(OH)_2$ into MgO [24]. For Mg–Ti solids, the presence of titanium seemed to favor such a transformation as evidenced by the shift of the peak to lower temperatures (in the 318–357 °C range).

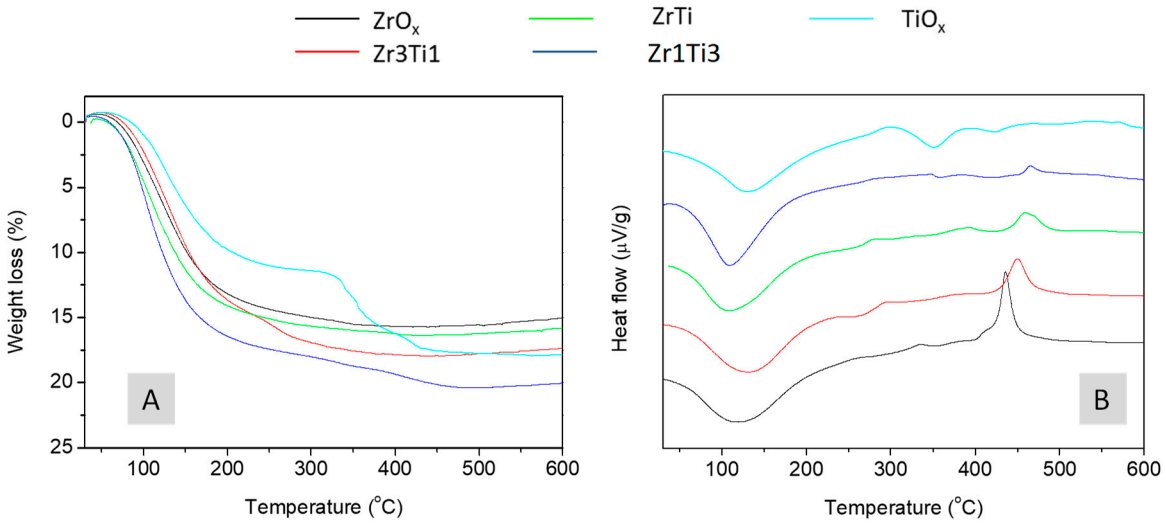

Figure 1. TG-DTA profiles of the precursor gels of the catalysts based on ZrO_x and TiO_x. Weight loss (**A**) and heat flow (**B**) profiles.

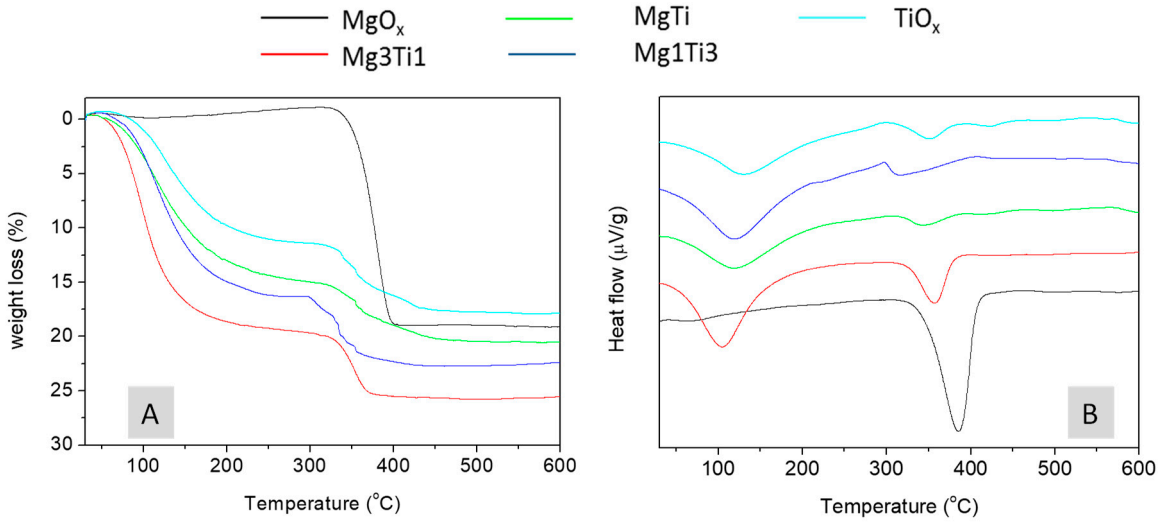

Figure 2. TG-DTA profiles of the precursor gels of catalysts based on MgO_x and TiO_x. Weight loss (**A**) and heat flow (**B**) profiles.

X-ray diffractograms of Zr-containing solids (Figure 3) showed evidence of their amorphous character, which was consistent with the TGA-DTA profiles; crystallization occurred at temperatures above 300 °C. In the case of MgO_x (Figure 3B), there were some peaks present due to the $Mg(OH)_2$ brookite structure. Those peaks were also evident in Mg3Ti1 solid whereas higher titanium contents resulted in the disappearance of brookite signals and the appearance of some new signals which could be assigned to MgO5Ti2 pseudobrookite.

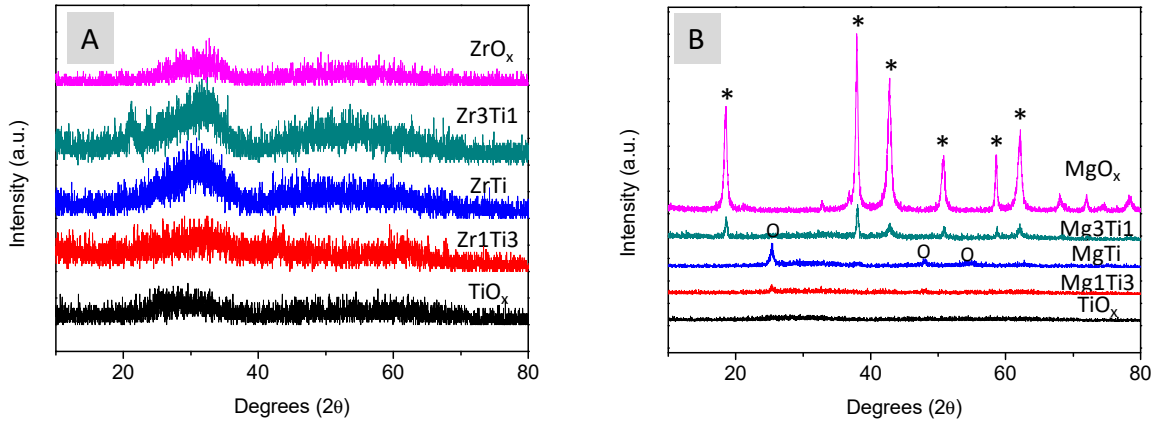

Figure 3. X-ray diffractograms of the different solids synthesized in the present work. Zr-Ti solids (**A**) and Mg-Ti systems (**B**). The corresponding pure compounds have also been included for the sake of comparison. * and ○ denote brookite and pseudobrookite phases, respectively.

Transmission electron microscopy (TEM) images of all the samples are represented in Figure 4. As can be seen in the central part of Figure 4, MgO_x, ZrO_x, and TiO_x exhibited quite different textures which allowed us to distinguish them in mixed solids.

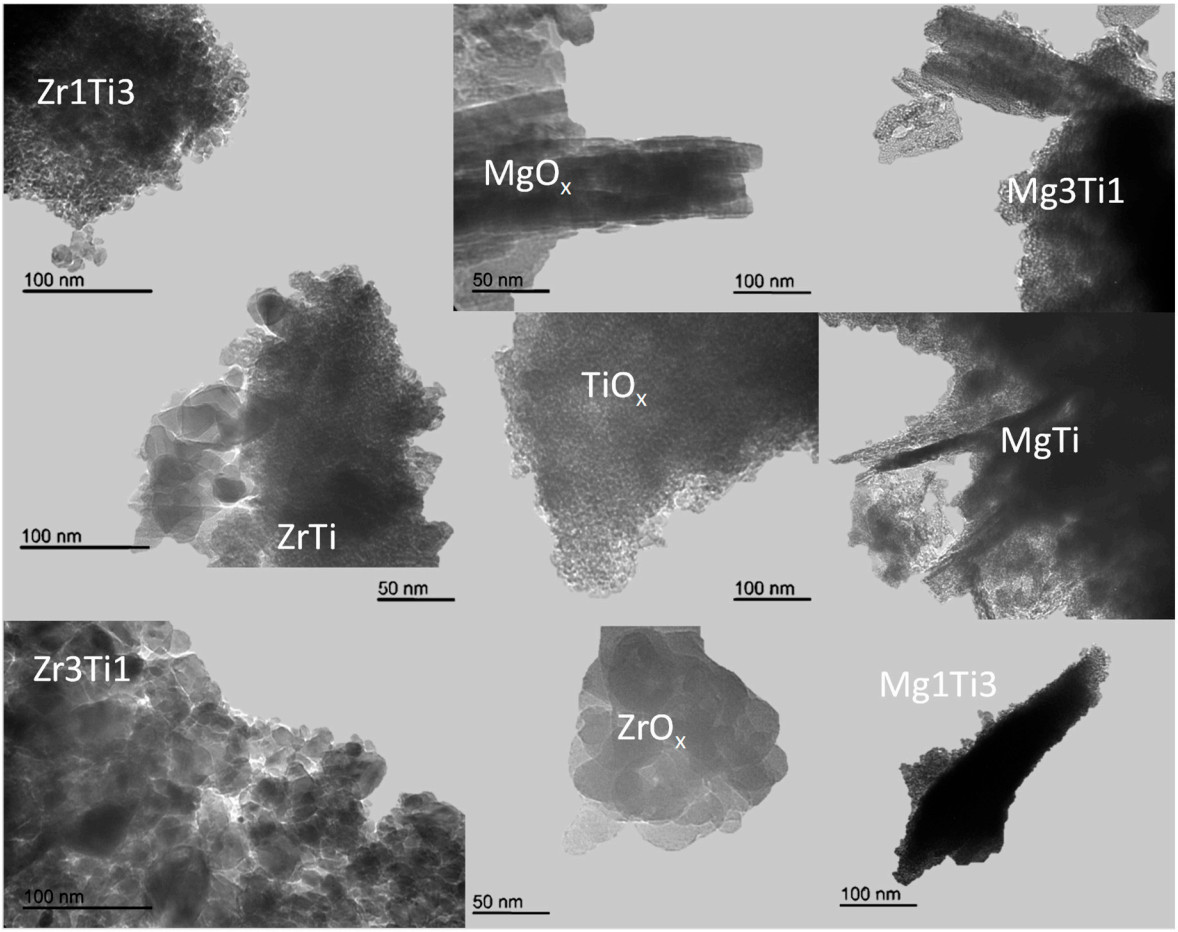

Figure 4. Transmission electron microscopy (TEM) images of the different solids.

X-ray photoelectron spectroscopy (XPS) profiles of Mg–Ti solids are represented in Figure 5. The signal for Mg1 in MgO_x presented two types of magnesium atoms. Moreover, as titanium content increased, there was a shift of signals to higher binding energies (from 1303.0 to 1303.8 eV for MgO_x

and Mg1Ti3, respectively). A similar trend was observed for the Ti(2p) signal, and the Ti2p3/2 signal shifted, in this case, to lower binding energies in the presence of magnesium (Ti2p3/2 signal at 458.4 and 458.1 eV for TiO_x and Ti3Mg1, respectively). These results suggest the existence of some Mg–Ti interaction in Mg–Ti solids.

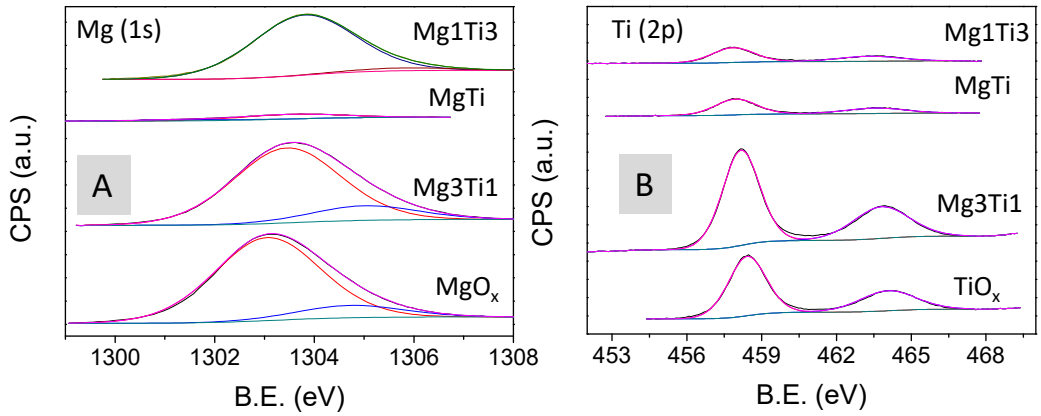

Figure 5. X-ray photoelectron spectroscopy (XPS) profiles of Mg(1s) (**A**) and Ti (2p) (**B**) in Mg–Ti solids.

As far as the Zr–Ti XPS profiles were concerned (Figure 6), there was suggestion of some Zr–Ti interaction as evidenced by the Zr3d and Ti2p signals shifting to higher and lower binding energy values, respectively, as the Ti content increased.

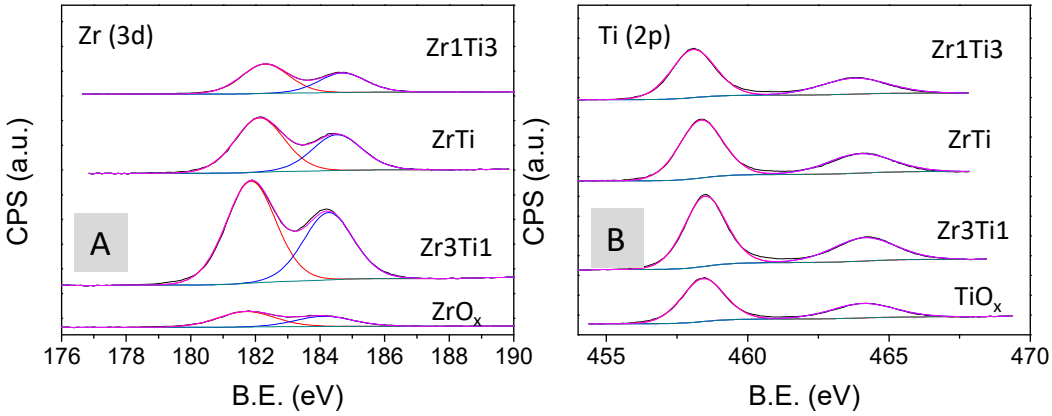

Figure 6. XPS profiles of Zr(3d) (**A**) and Ti (2p) (**B**) in Zr–Ti solids.

Surface acid–base characterization of the solids was carried out by TPD of pre-adsorbed CO_2 (basicity) and pyridine (acidity), and the main results are summarized in Table 2. As can be seen, ZrO_x exhibited a good balance between acid and basic sites (CO_2/py = 1.09), TiO_x was mainly acidic (CO_2/Py = 0.57) and MgO_x was a predominantly basic solid (CO_2/py = 3.39). As for the corresponding mixed solids, they all had an acid–base characteristic between the corresponding pure solids.

Table 2. Acid–base characteristics of the solids as determined by CO_2-TPD and Py-TPD, respectively.

Catalyst	μmol CO_2/g	μmol Py/g	CO_2/Py
ZrO_x	774	707	1.09
Zr3Ti1	728	753	0.97
ZrTi	658	921	0.71
Zr1Ti3	460	635	0.72
TiO_x	371	650	0.57
Mg1Ti3	508	622	0.82
MgTi	1126	616	1.83
Mg3Ti1	1142	354	3.22
MgO_x	1096	323	3.39

Complementary acid–base results could be obtained using the methylbutynol test reaction (Figure 7) which allow us to distinguish between acid, base, and acid–base pair sites.

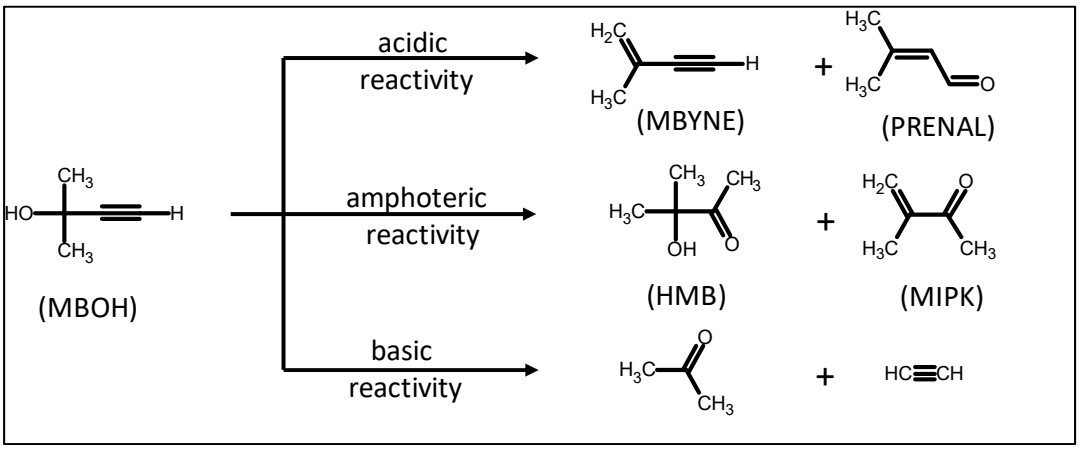

Figure 7. Overall reaction scheme as proposed by Lauron-Pernot et al. [25]. MBOH, 2-methyl-3-butyn-2-ol; MBYNE, 3-methyl-3-buten-1-yne; PRENAL, 3-methyl-2-buten-1-al; HMB, 3-hydroxy-3-methyl-2-butatone; MIPK, 3-methyl-3-buten-2-one.

As can be seen in Table 3, the methylbutynol (MBOH) test reaction confirmed the results found in the TPD studies of pre-adsorbed CO_2 and pyridine. Therefore, MgO_x mainly yielded acetone and acetylene (basic reactivity, 96.2% selectivity), TiO_x was mainly acidic (73.1% selectivity), and ZrO_x was predominantly amphoteric (53.4%) and mainly yielded 3-methyl-3-buten-2-one (MIPK). This was evidence for the presence of acid–base pair sites in ZrO_x.

Table 3. MBOH reaction. Comparison between selectivities of the pure oxides. The reaction conditions were as follows: microcatalytic pulse reactor; 20 mg catalyst, 200 °C, methylbutynol (MBOH) pulses of 0.5 μL (see experimental section).

Catalyst	Conversion (%)	S_{basic} (%)	S_{acid} (%)	$S_{amphoteric}$ (%)
MgO_x	5.6	96.2	3.8	0
TiO_x	1.0	12.3	73.1	14.6
ZrO_x	1.0	26.3	20.3	53.4

Further diffuse reflectance infrared Fourier transform (DRIFT) pyridine studies were performed on Zr–Ti solids to distinguish between Lewis and Brönsted acid sites (Figure 8). Peaks observed at 1443 and 1603 cm^{-1} were attributed to the presence of pyridine adsorbed on Lewis acid sites, whereas the band at ca. 1486 cm^{-1} could be due to adsorbed pyridine on both Lewis and Brönsted sites [26]. The signal at ca. 1534 cm^{-1} corresponded to pyridine on Brönsted acid sites [27]. An estimation

of the Lewis/Brönsted acid site ratio can be made by integrating signals using the molar extinction coefficients [28]. Therefore, Lewis/Brönsted values of 15.4 and 4.9 could be obtained for ZrO_x and TiO_x, respectively.

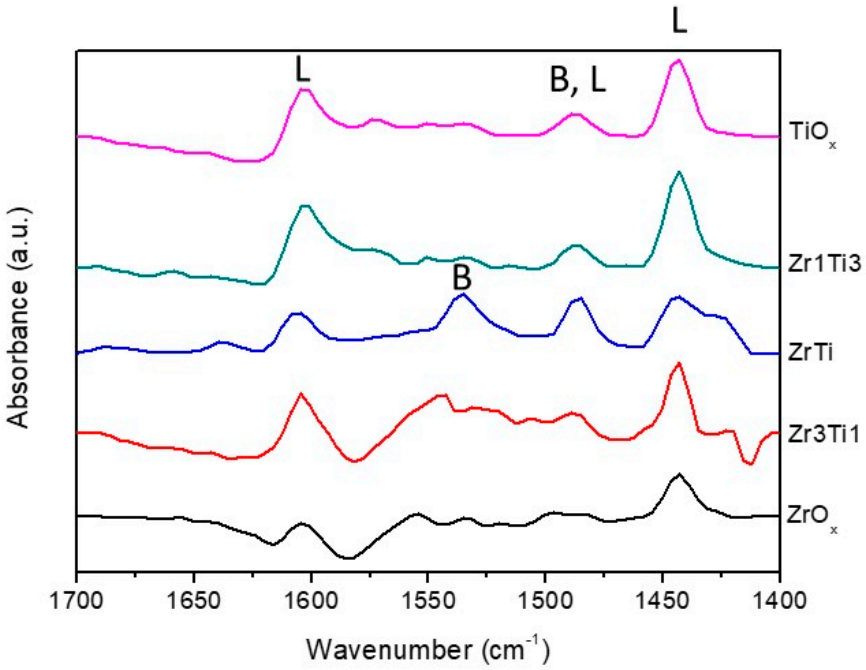

Figure 8. Diffuse reflectance infrared Fourier transform (DRIFT) studies of pyridine chemisorbed on the Zr–Ti solids. B and L stand for Brönsted and Lewis acid sites, respectively.

All in all, the acid–base studies indicated that MgO_x was mainly basic, ZrO_x was amphoteric, and TiO_x was acidic. Moreover, the highest Lewis/Brönsted site ratio corresponded to ZrO_x solids.

2.2. Catalytic Activity in Furfural Hydrogenation into Furfuryl Alcohol

The solids were then tested for liquid-phase MPV reduction of furfural to furfuryl alcohol (FUOL) using propan-2-ol as the hydrogen donor. The main results are summarized in Table 4.

Table 4. Results obtained for experiments under conventional (t = 20 h) and microwave (t = 2 h) heating on the different solids expressed in terms of conversion, selectivity to furfuryl alcohol (FUOL), and FUOL yield. The reaction conditions were as follows: 100 °C, molar propan-2-ol/furfural ratio of 10.8, and furfural/catalyst weight ratio of 5.8. Maximum microwave power was set at 300 W.

Catalyst	Conventional Heating			Microwave Heating		
	Conversion (%)	Selectivity FUOL (%)	Yield FUOL (%)	Conversion (%)	Selectivity FUOL (%)	Yield FUOL (%)
ZrO_x	50.1	90.4	45.3	27.6	96.8	26.7
Zr3Ti1	42.9	88.2	37.8	19.8	97.9	19.4
ZrTi	30.2	79.0	23.9	20.9	75.2	15.7
Zr1Ti3	22.3	80.5	18.0	17.1	79.5	13.6
TiO_x	16.2	68.7	11.1	7.4	53.5	4.0
Mg1Ti3	11.6	35.4	4.1	7.2	31.5	2.3
MgTi	13.4	46.6	6.3	8.6	47.8	3.1
Mg3Ti1	15.8	48.0	7.6	7.4	46.0	3.4
MgO_x	15.2	56.0	8.5	7.9	57.8	4.6

Firstly, the solids were tested under conventional heating. As can be seen, ZrO_x was the most active solid, followed by TiO_x and MgO_x. Both conversion and selectivity to furfuryl alcohol

dropped upon the introduction of titanium in Zr–Ti and Mg–Ti solids. This seems to indicate that the interaction evidenced by XPS (and also suggested by TGA-DTA profiles) is detrimental to activity. In the case of MgO_x, the main by-product was the condensation product between one molecule of furfural and one molecule of acetone. Microwave heating was also tested, and results for t = 2 h are given in Table 4. The reactions were indeed accelerated under microwave irradiation. For instance, for t = 2 h, conversions of 6.5% (not shown) and 27.6% as well as selectivities of 97.0 and 96.8% to furfuryl alcohol were achieved on ZrO_x under conventional and microwave heating, respectively. The results under microwave irradiation confirmed the observed activity trend in experiments under conventional heating.

The higher selectivity values (over 90%) found for ZrO_x could be ascribed to the existence of acid–base pair sites. As suggested by Komanoya et al. [29], there would be a synergistic effect of acid–base pair sites: base sites could activate methylene groups in propan-2-ol bonded to Lewis sites. A tentative reaction mechanism on those acid–base pair sites is presented in Figure 9. The better catalytic performance of ZrO_x as compared to TiO_x could also be explained as the result of Lewis sites being more active than Brönsted sites in the MPV reaction [30,31].

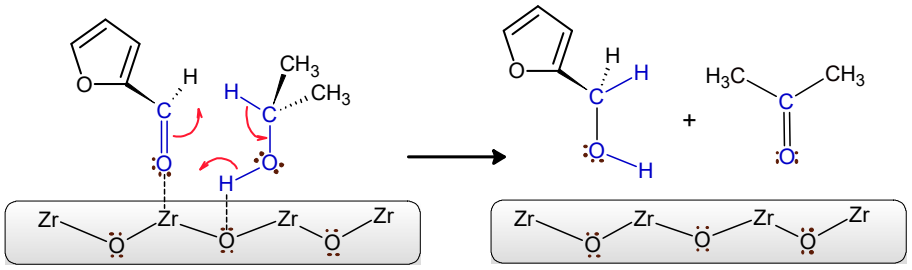

Figure 9. Suggested mechanism for furfural hydrogenation into furfuryl alcohol on acid–base pair sites in ZrO_x through transfer hydrogenation from propan-2-ol.

3. Materials and Methods

For the synthesis of the catalysts, the following compounds were used: aqueous solutions of ammonium hydroxide (5 N) (Fluka 318620-2L, Honeywell, Bucharest, Romania) and hydrochloric acid (1 M) (Fluka 318949-2L); propan-2-ol (Sigma-Aldrich 190764-2.5L, Merck KGaA, Darmstadt, Germany); hydrated zirconium(IV) oxynitrate (Sigma-Aldrich 346462, Merck KGaA, Darmstadt, Germany); magnesium nitrate hexahydrate (Sigma-Aldrich 237175-1KG, Merck KGaA, Darmstadt, Germany); and titanium isopropoxide (Sigma-Aldrich 20527-3, Merck KGaA, Darmstadt, Germany).

The synthesis of the catalysts was carried out by the sol–gel method [32], following previous studies in our research group [17,33–35].

Two types of mixed systems were synthesized: titanium gels with magnesium and titanium gels with zirconium, with different (Mg or Zr)/Ti molar ratios (0%, 25%, 50%, 75%, and 100%). The syntheses were carried out at a constant pH of 10 with magnetic stirring at 700 rpm. The pH was kept constant using a pump (Atlas syringe pump, Syrris, (Hertfordshire, UK), which added 5 N ammonium hydroxide or 1 M hydrochloric acid throughout the synthesis process. The precipitate was filtered, washed with water, dried at 120 °C overnight, and calcined at 200 °C for 8 h. After calcination, the catalysts were sieved (0.149 µm). The nomenclature of the solids was as follows: TiO_x, ZrO_x, and MgO_x for solids based on pure titanium, zirconium, and magnesium gels, respectively. For mixtures of gels, the nomenclature included the symbol of the metals followed by a number referring to their atomic ratio in the mixture. For instance, Mg3Ti1 indicates a magnesium–titanium system containing 75% Mg and 25% Ti (i.e., Mg/Ti atomic ratio of 3).

Thermogravimetric analyses (TGA) were performed on a Setaram SetSys 12 instrument (Caluire, France). A 20 mg amount of sample (precursor gels of the catalysts) was placed in an alumina crucible and heated at temperatures ranging from 30 to 600 °C (heating rate of 10 °C/min) under a synthetic air stream (50 mL/min) in order to measure weight loss, heat flow, and derivative weight loss.

X-ray photoelectron spectroscopy (XPS) data were recorded at the Central Service for Research Support (SCAI) of the University of Córdoba on 4 mm × 4 mm pellets of 0.5 mm thickness that were obtained by gently pressing the powered materials. The samples were outgassed to a pressure below about 2×10^{-8} Torr at 150 °C in the instrument pre-chamber to remove chemisorbed volatile species. The main chamber of the Leibold-Heraeus LHS10 spectrometer used, which is capable of operating down to less than 2×10^{-9} Torr, was equipped with a EA-200MCD hemispherical electron analyzer with a dual X-ray source using Al Kα (hυ = 1486.6 eV) at 120 W and 30 mA. C (1 s) was used as the energy reference (284.6 eV).

Transmission electron microscopy (TEM) images were obtained at the Central Service for Research Support (SCAI) of the University of Córdoba using a JEOL JEM 1400 microscope available at SCAI. The samples were mounted on 3 mm holey carbon copper grids.

X-ray patterns of the samples in the 10−80° (2θ) range was registered in a D8 Advanced Diffractometer (Bruker AXS) equipped with a Lynxeye detector.

Surface areas of solids were obtained from nitrogen adsorption-desorption isotherms obtained at liquid nitrogen temperature on a Micromeritics ASAP-2010 instrument following the Brunnauer–Emmett–Teller (BET) method. All samples were degassed to 0.1 Pa at 120 °C before measurement.

Surface basicity of the catalysts was determined on a Micromeritics Autochem II instrument by thermal programmed desorption of pre-absorbed CO_2 (TPD-CO_2) with TCD detection. An amount of 100 mg of each catalyst was loaded into a reactor of 10 mm ID and placed in a furnace. Solids were cleaned with an Ar stream (20 mL/min) by heating to 200 °C at a rate of 10 °C/min for 60 min and then cooled down to 40 °C. At that temperature, the catalysts were saturated with the probe molecule using 5% CO_2/Ar flow at 20 mL/min for 60 min. After saturation, physisorbed CO_2 was removed by a flowing Ar stream for 30 min (20 mL/min). Then, the temperature-programmed desorption of chemisorbed CO_2 was carried out by ramping the temperature from 40 to 200 °C (heating rate 5 °C/min) and holding the final temperature for 60 min. The amount of CO_2 adsorbed was determined from a calibration graph constructed from the injection of variable volumes of 5% CO_2/Ar.

The surface acidity of the catalysts was determined by thermal programmed desorption of pre-adsorbed pyridine (TPD-PY) with TCD detection. A 30 mg amount of sample was introduced in a 10 mm ID reactor that was placed inside an oven. The solids were cleaned under a He flow (75 mL/min) by heating to 200 °C at a rate of 10 °C/min and then cooled down to 50 °C. At that temperature, the solids were exposed for 30 min to a pyridine-saturated He flow. After saturation, physisorbed pyridine was removed by flowing a pure He stream for 60 min (75 mL/min). Then, the temperature-programmed desorption of chemisorbed pyridine was carried out by ramping the temperature from 50 to 200 °C (heating rate 10 °C/min) and holding the final temperature for 30 min. Desorbed pyridine was quantified against a calibration graph constructed from variable volumes of pyridine injected.

Complementary studies using diffuse reflectance infrared Fourier transform (DRIFT) spectra of adsorbed pyridine were carried out on a FTIR instrument (Bomem MB-3000, ABB Corporate, Zurich, Switzerland) equipped with an "environmental chamber" (Spectra Tech, Jefferson Court, Oak Ridge, TN, USA) placed in a diffuse reflectance attachment (Spectra Tech, Collector). A resolution of 8 cm^{-1} was used with 256 scans averaged to obtain a spectrum from 4000 to 400 cm^{-1}. In each measurement, the reference was the same sample after heating at 150 °C. Pyridine adsorption was carried out at 150 °C for 45 min to allow the saturation of the catalyst surface. The physisorbed pyridine was then cleaned with a N_2 flow (50 mL/min) and its spectrum was registered.

The MBOH test reaction was carried out as described elsewhere [36]. A microcatalytic pulse reactor (1/8 in i.d. quartz tubular reactor) was placed in the injection port of a gas chromatograph (GC System 7890A, Agilent Technologies, Santa Clara, CA, USA). The reactor was packed with alternating layers of quartz wool with the catalyst (20 mg) placed between them. Prior to each run,

the catalyst was pre-treated in the reactor at 200 °C for 2 h under nitrogen (75 mL/min). MBOH pulses of 0.5 μL were then carried out.

The MPV reaction of furfural was carried out under conventional heating in a Carousel 12 Plus™ Reaction Station, Discovery Technologies, and reactions under microwaves were carried out in a CEM-DISCOVER apparatus with PC control. In both cases, temperature was 100 °C. Maximum microwave power was set at 300 W. The reactions by conventional heating were carried out with 100 mg of catalyst, 5 mL of propan-2-ol, and 0.5 mL of furfural over 20 h; the reactions in the microwave oven kept the same catalyst, propan-2-ol, and furfural ratios at a volume of reaction of 2 mL with a reaction time of 2 h. Analysis of reaction products was carried out by gas chromatography (GC-FID System 7890A, Agilent Technologies, equipped with a HP-5 chromatographic column) using the corresponding calibration graphs.

4. Conclusions

Several solids consisting of pure magnesium, zirconium, titanium, and mixed magnesium–titanium as well as zirconium–titanium gels were obtained through the sol–gel process and calcined at 200 °C. The presence of titanium retarded the crystallization of zirconium oxide whereas transformation of $Mg(OH)_2$ into MgO was favored in the presence of titanium. XPS results also suggested the existence of some Mg–Ti and Zr–Ti interaction in mixed gels. In regard to the acid–base properties as determined from the TPD of pre-adsorbed pyridine and CO_2, the ZrO_x system exhibited a good balance between acid and base sites, whereas TiO_x and MgO_x were predominantly acidic and basic, respectively. The MBOH test reaction evidenced the presence of acid–base pair sites in ZrO_x, and pyridine DRIFT studies showed that acid sites in ZrO_x were mainly of the Lewis type whereas both Brönsted and Lewis sites were present in TiO_x and Zr–Ti mixed solids. The most active and selective catalyst in the MPV reduction of furfural to furfuryl alcohol was ZrO_x whereas both parameters decreased in Zr–Ti solids as the titanium content increased. These results suggest that acid–base pair sites are particularly active in MPV reduction and that Lewis acid sites are more active than Brönsted acid ones. The same reactivity order was found for the reactions under microwave irradiation which led to an acceleration of the process as compared to conventional heating.

Author Contributions: A.M., J.H.-C. and F.J.U. conceived and designed the experiments; J.H.-C., A.P. and M.J.C.-R. performed the experiments; J.H.-C., A.P. and M.J.C.-R. analyzed the data; J.H.-C., A.M. and F.J.U. wrote the paper.

Funding: This research was funded by the Ramón Areces Foundation.

Acknowledgments: The scientific support from the Central Service for Research Support (SCAI) at the University of Cordoba is acknowledged.

Conflicts of Interest: The authors declare no conflict of interest.

References

1. Chheda, J.N.; Huber, G.W.; Dumesic, J.A. Liquid-phase catalytic processing of biomass-derived oxygenated hydrocarbons to fuels and chemicals. *Angew. Chem. Int. Ed.* **2007**, *46*, 7164–7183. [CrossRef] [PubMed]
2. Turhollow, A.; Perlack, R.; Eaton, L.; Langholtz, M.; Brandt, C.; Downing, M.; Wright, L.; Skog, K.; Hellwinckel, C.; Stokes, B.; et al. The updated billion-ton resource assessment. *Biomass Bioenergy* **2014**, *70*, 149–164. [CrossRef]
3. Bozell, J.J.; Petersen, G.R. Technology development for the production of biobased products from biorefinery carbohydrates-the US Department of Energy's "Top 10" revisited. *Green Chem.* **2010**, *12*, 539–554. [CrossRef]
4. Mamman, A.S.; Lee, J.-M.; Kim, Y.-C.; Hwang, I.T.; Park, N.-J.; Hwang, Y.K.; Chang, J.-S.; Hwang, J.-S. Furfural: Hemicellulose/xylosederived biochemical. *Biofuels Bioprod. Biorefin.* **2008**, *2*, 438–454. [CrossRef]
5. Chatterjee, C.; Pong, F.; Sen, A. Chemical conversion pathways for carbohydrates. *Green Chem.* **2015**, *17*, 40–71. [CrossRef]
6. Corma, A.; Iborra, S.; Velty, A. Chemical Routes for the Transformation of Biomass into Chemicals. *Chem. Rev.* **2007**, *107*, 2411–2502. [CrossRef] [PubMed]

7. Rothe, M.; Bauer, K.; Garbe, D. *Common Fragrance and Flavour Materials. Preparation, Properties and Uses*; VCH Verlagsgesellschaft mbH: Weinheim, Germany, 1985.
8. Liu, H.; Huang, Z.; Zhao, F.; Cui, F.; Li, X.; Xia, C.; Chen, J. Efficient hydrogenolysis of biomass-derived furfuryl alcohol to 1,2-and 1,5-pentanediols over a non-precious Cu-$Mg_3AlO_{4.5}$ bifunctional catalyst. *Catal. Sci. Technol.* **2016**, *6*, 668–671. [CrossRef]
9. Rao, R.; Dandekar, A.; Baker, R.T.K.; Vannice, M.A. Properties of Copper Chromite Catalysts in Hydrogenation Reactions. *J. Catal.* **1997**, *171*, 406–419. [CrossRef]
10. Sang, S.; Wang, Y.; Zhu, W.; Xiao, G. Selective hydrogenation of furfuryl alcohol to tetrahydrofurfuryl alcohol over Ni/γ-Al_2O_3 catalysts. *Res. Chem. Intermed.* **2017**, *43*, 1179–1195. [CrossRef]
11. Taylor, M.J.; Durndell, L.J.; Isaacs, M.A.; Parlett, C.M.A.; Wilson, K.; Lee, A.F.; Kyriakou, G. Highly selective hydrogenation of furfural over supported Pt nanoparticles under mild conditions. *Appl. Catal. B Environ.* **2016**, *180*, 580–585. [CrossRef]
12. Thompson, S.T.; Lamb, H.H. Palladium–Rhenium Catalysts for Selective Hydrogenation of Furfural: Evidence for an Optimum Surface Composition. *ACS Catal.* **2016**, *6*, 7438–7447. [CrossRef]
13. Meerwein, H.; Schmidt, R. Ein neues Verfahren zur Reduktion von Aldehyden und Ketonen. *Justus Liebigs Annalen der Chemie* **1925**, *444*, 221–238. [CrossRef]
14. Ooi, T.; Ichikawa, H.; Maruoka, K. Practical Approach to the Meerwein–Ponndorf–Verley Reduction of Carbonyl Substrates with New Aluminum Catalysts. *Angew. Chem.* **2001**, *113*, 3722–3724. [CrossRef]
15. Ivanov, V.; Bachelier, J.; Audry, F.; Lavalley, J.C. Study of the Meerwein-Pondorff-Verley Reaction Between Ethanol and Acetone on Various Metal-Oxides. *J. Mol. Catal.* **1994**, *91*, 45–59. [CrossRef]
16. Montes, V.; Miñambres, J.F.; Khalilov, A.N.; Boutonnet, M.; Marinas, J.M.; Urbano, F.J.; Maharramov, A.M.; Marinas, A. Chemoselective hydrogenation of furfural to furfuryl alcohol on ZrO_2 systems synthesized through the microemulsion method. *Catal. Today* **2018**, *306*, 89–95. [CrossRef]
17. Axpuac, S.; Aramendía, M.A.; Hidalgo-Carrillo, J.; Marinas, A.; Marinas, J.M.; Montes-Jiménez, V.; Urbano, F.J.; Borau, V. Study of structure-performance relationships in Meerwein-Ponndorf-Verley reduction of crotonaldehyde on several magnesium and zirconium-based systems. *Catal. Today* **2012**, *187*, 183–190. [CrossRef]
18. Antunes, M.M.; Lima, S.; Neves, P.; Magalhães, A.L.; Fazio, E.; Neri, F.; Pereira, M.T.; Silva, A.F.; Silva, C.M.; Rocha, S.M.; et al. Integrated reduction and acid-catalysed conversion of furfural in alcohol medium using Zr,Al-containing ordered micro/mesoporous silicates. *Appl. Catal. B Environ* **2016**, *182*, 485–503. [CrossRef]
19. Iglesias, J.; Melero, J.A.; Morales, G.; Moreno, J.; Segura, Y.; Paniagua, M.; Cambra, A.; Hernandez, B. Zr-SBA-15 Lewis Acid Catalyst: Activity in Meerwein Ponndorf Verley Reduction. *Catalysts* **2015**, *5*, 1911–1927. [CrossRef]
20. Iglesias, J.; Melero, J.A.; Morales, G.; Paniagua, M.; Hernández, B. Dehydration of Xylose to Furfural in Alcohol Media in the Presence of Solid Acid Catalysts. *ChemCatChem* **2016**, *8*, 2089–2099. [CrossRef]
21. Kim, M.S.; Simanjuntak, F.S.H.; Lim, S.; Jae, J.; Ha, J.-M.; Lee, H. Synthesis of alumina–carbon composite material for the catalytic conversion of furfural to furfuryl alcohol. *J. Ind. Eng. Chem.* **2017**, *52*, 59–65. [CrossRef]
22. Lopez-Asensio, R.; Cecilia, J.A.; Jimenez-Gomez, C.P.; Garcia-Sancho, C.; Moreno-Tost, R.; Maireles-Torres, P. Selective production of furfuryl alcohol from furfural by catalytic transfer hydrogenation over commercial aluminas. *Appl. Catal. A Gen.* **2018**, *556*, 1–9. [CrossRef]
23. Stefanic, G.; Music, S.; Popovic, S.; Sekulic, A. FT-IR and laser Raman spectroscopic investigation of the formation and stability of low temperature t-ZrO_2. *J. Mol. Struct.* **1997**, *408–409*, 391–394. [CrossRef]
24. Formosa, J.; Chimenos, J.M.; Lacasta, A.M.; Haurie, L. Thermal study of low-grade magnesium hydroxide used as fire retardant and in passive fire protection. *Thermochim. Acta* **2011**, *515*, 43–50. [CrossRef]
25. Lauron-Pernot, H.; Luck, F.; Popa, J.M. Methylbutynol: A new and simple diagnostic tool for acidic and basic sites of solids. *Appl. Catal.* **1991**, *78*, 213. [CrossRef]
26. Osman, A.I.; Abu-Dahrieh, J.K.; Rooney, D.W.; Halawy, S.A.; Mohamed, M.A.; Abdelkader, A. Effect of precursor on the performance of alumina for the dehydration of methanol to dimethyl ether. *Appl. Catal. B Environ.* **2012**, *127*, 307–315. [CrossRef]
27. Lu, J.; Kosuda, K.M.; Van Duyne, R.P.; Stair, P.C. Surface Acidity and Properties of TiO_2/SiO_2 Catalysts Prepared by Atomic Layer Deposition: UV-visible Diffuse Reflectance, DRIFTS, and Visible Raman Spectroscopy Studies. *J. Phys. Chem. C* **2009**, *113*, 12412–12418. [CrossRef]

28. Emeis, C.A. Determination of Integrated Molar Extinction Coefficients for Infrared Absorption Bands of Pyridine Adsorbed on solid Acid Catalysts. *J. Catal.* **1993**, *141*, 347–354. [CrossRef]
29. Komanoya, T.; Nakajima, K.; Kitano, M.; Hara, M. Synergistic Catalysis by Lewis Acid and Base Sites on ZrO_2 for Meerwein-Ponndorf-Verley Reduction. *J. Phys. Chem. C* **2015**, *119*, 26540–26546. [CrossRef]
30. Guo, Z.-K.; Hong, Y.-C.; Xu, B.-Q. Transfer hydrogenation of cinnamaldehyde with 2-propanol on Al_2O_3 and SiO_2-Al_2O_3 catalysts: Role of Lewis and Brönsted acidic sites. *Catal. Sci. Technol.* **2017**, *7*, 4511–4519. [CrossRef]
31. Miñambres, J.F.; Aramendía, M.A.; Marinas, A.; Marinas, J.M.; Urbano, F.J. Liquid and gas-phase Meerwein–Ponndorf–Verley reduction of crotonaldehyde on ZrO_2 catalysts modified with Al_2O_3, Ga_2O_3 and In_2O_3. *J. Mol. Catal. A Chem.* **2011**, *338*, 121–129. [CrossRef]
32. Debecker, D.P.; Mutin, P.H. Non-hydrolytic sol-gel routes to heterogeneous catalysts. *Chem. Soc. Rev.* **2012**, *41*, 3624–3650. [CrossRef] [PubMed]
33. Minambres, J.F.; Marinas, A.; Marinas, J.M.; Urbano, F.J. Activity and deactivation of catalysts based on zirconium oxide modified with metal chlorides in the MPV reduction of crotonaldehyde. *Appl. Catal. B Environ.* **2013**, *140*, 386–395. [CrossRef]
34. Minambres, J.F.; Marinas, A.; Marinas, J.M.; Urbano, F.J. Chemoselective crotonaldehyde hydrogen transfer reduction over pure and supported metal nitrates. *J. Catal.* **2012**, *295*, 242–253. [CrossRef]
35. Aramendia, M.A.; Borau, V.; Jimenez, C.; Marinas, J.M.; Ruiz, J.R.; Urbano, F.J. Influence of the preparation method on the structural and surface properties of various magnesium oxides and their catalytic activity in the Meerwein-Ponndorf-Verley reaction. *Appl. Catal. A Gen.* **2003**, *244*, 207–215. [CrossRef]
36. Aramendia, M.A.; Borau, V.; Garcia, I.M.; Jimenez, C.; Marinas, A.; Marinas, J.M.; Porras, A.; Urbano, F.J. Comparison of Different Organic Test Reaction over Acid-Base Catalysts. *Appl. Catal. A Gen.* **1999**, *184*, 115–125. [CrossRef]